Osteogenic potential of sol-gel bioactive glasses containing manganese

Breno Rocha Barrioni[1,*], Elizabeth Norris[2], Siwei Li[2], Parichart Naruphontjirakul[2,3], Julian R. Jones[2] and Marivalda de Magalhães Pereira[1]

[1]Department of Metallurgical Engineering and Materials, Federal University of Minas Gerais, School of Engineering, Belo Horizonte, MG, Brazil

[2]Department of Materials, Imperial College London, South Kensington, London, SW7 2AZ, UK

[3]Biological Engineering Program, King Mongkut's University of Technology Thonburi, Thailand

*Corresponding author. Tel.: +5531984764001

E-mail addresses: brenobarrionibh@hotmail.com (B. R. Barrioni); e.norris14@imperial.ac.uk (E. Norris); siwei.li@imperial.ac.uk (S. Li); parichart.nar@kmutt.ac.th (P. Naruphontjirakul); julian.r.jones@imperial.ac.uk (J. R. Jones); mpereira@demet.ufmg.br (M. M. Pereira)

Abstract We report that the release of manganese ions from bioactive glass provoked human mesenchymal stem cell (hMSC) differentiation down a bone pathway, whereas hMSCs exposed to the Mn-free glass did not differentiate. Bioactive glasses (BGs) are widely used for bone regeneration, and allow the incorporation of different ions with therapeutic properties into the glass network. Amongst the different ions with therapeutic benefits, manganese (Mn) has been shown to influence bone metabolism and activate human osteoblasts integrins, improving cell adhesion, proliferation and spreading. Mn has also been incorporated into bioceramics as a therapeutic ion for improved osteogenesis. Here, up to 4.4 mol% MnO was substituted for CaO in the 58S composition (60 mol% SiO_2, 36 mol% CaO, 4 mol% P_2O_5) and its effects on the glass properties and capability to influence the osteogenic differentiation were evaluated. Mn-containing BGs with amorphous structure, high specific surface area and nanoporosity were obtained. The presence of Mn^{2+} species was confirmed by X-ray photoelectron spectroscopy (XPS). Mn-containing BGs presented no cytotoxic effect on human mesenchymal stem cells (hMSCs) and enabled sustained ion release in culture medium. hMSCs osteogenic differentiation stimulation and influence on the mineralisation process was also confirmed through the alkaline phosphatase (ALP) activity, and expression of osteogenic differentiation markers, such as collagen type I, osteopontin and osteocalcin, which presented higher expression in the presence of Mn-containing samples compared to control. Mn incorporation offers great promise for obtaining glasses with superior properties for bone tissue regeneration.

Keywords: bioactive glass; sol-gel; manganese; stem cells; osteogenic differentiation

1 Introduction

45S5 Bioglass® was first synthesised by Larry Hench in 1969 as the first inorganic material to bond with living bone without triggering scar tissue formation after implantation [1]. This led to the field of bioactive materials; moving away from the traditional view that implant medical devices should be inert and simply replace old damaged tissue, instead active tissue regeneration is preferred [2]. Bioactive glass (BG) compositions, such as the original 45S5, undergo specific reactions at their surface following the glass dissolution resulting in the formation of a hydroxycarbonate apatite (HCA) layer, which is similar to the bone mineral phase and can interact with collagen fibrils and bond with bone [1,3]. The glass dissolution products can also increase cell proliferation and stimulate bone regeneration at a genetic level [4]. BG based materials activate rapid bone regeneration and are already widely used as synthetic bone grafts in orthopaedic and dental applications [3].

While the role of bioactive glasses on osteoblasts is well documented, their effect on stem cells is less clear. Osteogenic differentiation of hMSCs in contact with Bioglass® 45S5 was measured [5] but the glass did not stimulate the alkaline phosphatase (ALP) activity of hMSCs of five donors [6]. Dissolution products of sol-gel 58S BG (60 mol% SiO_2, 36 mol% CaO, 4 mol% P_2O_5) enhanced the differentiation of *murine* embryonic stem cells to osteogenic cells, indicated by increased mineralized nodule formation, ALP activity, and osteoblast-associated (*runx2*/*cbfa-1*) gene expression [7]. Dissolution products of a sol-gel glass with higher phosphate content (60 mol% SiO_2, 28 mol% CaO, 12 mol% P_2O_5) also provoked mineralisation and increased mRNA expression of the osteogenic differentiation markers ALP, osteopontin and osteonectin from human dental pulp stem cells (hDPSCs) [8]. Here, the aim is to add to the data on how bioactive glasses can influence hMSC differentiation.

Sol-gel derived glasses usually present enhanced bioactivity when compared to the melt derived glasses with similar composition, due to their high surface area and inherent nanoporosity improving their dissolution process [9]. A wide range of glass morphologies can be obtained through sol-gel, such as nano and micro structures, fibres, and coatings. Due to the processing versatility, different glass compositions can be obtained, allowing the incorporation of several ions with therapeutic properties [10]. For example, strontium-containing BGs are being evaluated for osteoporosis treatment, as it could inhibit osteoclast differentiation while improving osteoblasts activity [11,12]. Replacing some of the Ca in BGs for Sr enhanced osteogenic response of osteoblasts [13] and promoted up-regulation of osteogenic differentiation genes in bone marrow derived stem cells

(hMSCs) *in vitro,* such as osteocalcin and alkaline phosphatase [14,15] and promoted osteoconduction *in vivo* [16]. Sr containing BGs provoked up-regulation of genes in hMSCs, such as osteopontin, and bone morphogenetic protein 2 (*bmp2*), activating the sterol synthesis pathway and modified membrane cholesterol and the lipid rafts [17]. Nanoparticles containing as little as 4.4 mol% SrO (90.6 mol% SiO_2, 5.0 mol% CaO, 4.4% mol% SrO) stimulated hMSCs to differentiated down an osteogenic route, where Sr-free nanoparticles did not differentiate [18].

Ions such as silver and gallium have demonstrated antibacterial properties [19,20], whereas cobalt can stimulate new blood vessel formation [21,22], similar effect observed in copper-doped glasses [23]. Those ions can be released during the glass dissolution process, improving the glass biological effect.

Amongst the different ions with therapeutic properties, Mn has attracted attention in recent years for incorporation in different bioceramics. In human osteoblast culture, Mn^{2+} has been shown to influence integrin activity that mediate interactions with the extracellular matrix (ECM) and are essential for cell adhesion, spreading and proliferation [24]. Mn ions are also involved in the ECM and plasmatic membrane protein synthesis, such as collagen, playing key roles in bone and other connective tissue formation [25]. Mn ions can also influence bone and muscle metabolism and affect bone mass maintenance [26], and have been proposed as means to improve bone regeneration. Higher osteoblast-like cell-adhesion was observed on Mn-containing hydroxyapatites [27], compared to synthetic HA, and tricalcium phosphates containing this ion presented higher bone mineralisation rates [28]. An increase in the osteogenesis-related gene expression and collagen deposition rate was observed in Mn-containing titanium implants exposed to rat bone marrow mesenchymal stem cells [29]; an increased antibacterial activity was also observed in multifunctional materials containing this ion [29,30]. Melt-derived BGs containing Mn promoted alkaline phosphatase activity (ALP) and BMP expression in osteoblast culture, and presented good osteoblast proliferation and spreading [25]. Although limited work in sol-gel derived BGs containing Mn is reported, sol-gel derived mesoporous BG nanoparticles were previously obtained, which showed *in vitro* bioactivity and also antibacterial effect [31]. We have also previously demonstrated that different Mn-containing BG microparticle compositions derived from the sol-gel process can be obtained, with HCA layer formation in simulated body fluid (SBF) within less than 1 day [32]. An ion release study showed that Mn ion level could be adjusted [32] to lower concentrations than 0.1 mM, reported to inhibit osteoblasts proliferation and spreading [24], and contributing to the promise of such a composition

as a potential strategy to obtain superior materials for bone repair. Further evaluation remains necessary to confirm the Mn potential on the osteogenic differentiation and bone mineralisation.

Here, sol-gel-derived bioactive glasses in the SiO_2-CaO-P_2O_5-MnO containing different Mn contents were synthesised, and the effect of Mn incorporation on the glass structure, textural properties and chemical composition was investigated. The controlled ion release capability was assessed through culture medium dissolution studies. The effect of the BGs ionic products on human bone marrow-derived mesenchymal stem cells (hMSCs) osteogenic differentiation and bone mineralisation was investigated. The expression of proteins associated with bone matrix formation, such as collagen type I and ALP, and markers of the mineralisation stage (osteopontin and osteocalcin expression, and calcium nodule formation) were evaluated, in order to confirm Mn incorporation in sol-gel glasses as a strategy to obtain materials with therapeutic benefits for tissue engineering.

2 Materials and Methods

2.1 Synthesis of bioactive glass microparticles

The sol-gel method was applied to obtain BG microparticles as previously reported [33] based on the 58S nominal composition (60 mol% SiO_2, 36 mol% CaO, 4 mol% P_2O_5). Unless otherwise stated, reagents used in this work were obtained from Sigma-Aldrich (UK). TEOS (tetraethyl orthosilicate 98%) and TEP (triethyl phosphate 99%) were added to nitric acid (2 M) and deionized water, at a molar ratio H_2O/TEOS (R ratio) of 12. The reagents were mixed for 1 h with magnetic stirring (room temperature). After that, calcium nitrate tetrahydrate ($Ca(NO_3)_2.4H_2O$) was dissolved in the sol, and magnetic stirring was maintained for another 1 h. Mn-containing samples were obtained by partial replacement of the Ca content on the BG samples. This was achieved by dissolving the Mn precursor (manganese nitrate hydrate, $Mn(NO_3)_2.xH_2O$) in the sol prior to the Ca precursor dissolution. The obtained gel was placed in a sealed polytetrafluoroethylene (PTFE) large screw top container and aged for 72 h at 60 °C. Then, the container was opened and dried with a rate of 10 °C / 24 h, until reaching 120 °C and held for 24 h. Samples were thermally treated at 650 °C for 3 h (2 °C/min). Finally, samples were ground and sieved, and the particle fraction below 150 µm evaluated in this work. The nominal compositions in the samples obtained in this work are listed in Table 1.

2.2 BG characterization

Chemical composition

Chemical evaluation was performed using the acid digestion method. For this process, 50 mg of each sample, and 250 mg of anhydrous lithium metaborate (80% w/w) and lithium tetraborate (20% w/w) (*Spectroflux 100B*, Alfa Aesar) were mixed in a platinum crucible, and then fused (30 min) in a furnace at 1050 °C. Then, after cooling, samples were fully dissolved in nitric acid (2 M). Concentrations of Si, Ca, P and Mn in each sample were determined via the inductively coupled plasma-optical emission spectrometer (ICP-OES - Thermo Scientific iCaP 6000 series). Finally, the proportions of SiO_2, CaO, P_2O_5 and MnO in each sample were calculated.

Structural evaluation

Fourier transform infrared spectroscopy (FTIR) was performed on a Thermo Scientific Nicolet iS10 equipped with Attenuated Total Reflectance (ATR). The spectra were collected from 400 to 4000 cm^{-1}, at 4 cm^{-1} resolution and 64 scans collected per spectrum. X-ray diffraction (XRD) patterns were obtained from 7 to 70° (2θ) and 0.02 step size (without spinning) in a Bruker D2 phaser using a CuKα radiation source. A K-Alpha$^+$ system (Thermo Scientific) operating at 2 x 10^{-9} mbar was applied on the X-ray photoelectron spectroscopy (XPS) analysis using a micro-fused and monochromated Al Kα X-ray source (hv = 1486.6 eV). A 180° double focusing hemispherical analyser incorporated with a 2D detector was used, with 12 kV anode bias and 6 mA emission current of the X-ray source. A flood gun was used to reduce sample charging, which was corrected using the C 1s core line at 285.0 eV. The X-ray spot size was 400 µm, 200 eV pass energy for survey and 20 eV pass energy for core level evaluation. Data were evaluated using the Avantage XPS software. High-resolution XPS scans were performed for Si 2p, O 1s and Mn 2p core-levels.

Textural properties

A Quantachrome Autosorb AS-6 multi-station equipment was used for nitrogen sorption analysis. Samples were first degassed at 200 °C for 24 h and subsequently evaluated by nitrogen sorption analysis (40 adsorptions and 40 desorption points). The specific surface area was evaluated in absorption data points in the P/P_0 range of 0.01 to 0.30 applying the Brunauer-Emmett-Teller (BET) method [34]. The pore diameter distribution was evaluated using the desorption curves and the Barret-Joyner-Halenda (BJH) method [35].

DMEM dissolution study

Samples (75 mg) were immersed in 50 mL DMEM (Dulbecco Modified Eagle Medium, Gibco) in an airtight polypropylene container and incubated at 37 °C under agitation (120 rpm), according to the conditions proposed by Maçon et al. [36]. Solution (1 mL) was collected at successive time points (0, 4, 8, 24 and 72 h) and then replaced by 1 mL fresh DMEM solution in each container. Each collected aliquot was diluted in 2 M nitric acid, syringe filtered (0.22 µm) and the Si, Ca, P and Mn ionic concentration measured by ICP-OES. Tests were performed in triplicate, and results are expressed as mean ± standard deviation.

2.3 Cytotoxic analysis

Ionic product media

Samples were incubated in α-MEM at 1.5 mg.mL^{-1} ratio, 37 °C and 120 rpm agitation for 4 h. The medium containing the glass ionic product was then filtered (0.22 µm) and supplemented with 10% fetal bovine serum (FBS) (v/v), 100 U.mL^{-1} penicillin and 100 µg.mL^{-1} streptomycin (Thermo Fisher Scientific, UK).

Cell viability

Human bone marrow-derived mesenchymal stem cells (ATCC® PCS-500-012™) were used for the cell viability study. In this process, cells were expanded in T-125 cell culture flasks)Corning®; Sigma-Aldrich, UK(at 5% CO_2, fully humidified atmosphere and 37 °C in basal condition (α-MEM supplemented with 10% fetal bovine serum (FBS) (v/v), 100 U.mL^{-1} penicillin and 100 µg.mL^{-1} streptomycin; Thermo Fisher Scientific, UK). A concentration of 5 x 10^4 cells.mL^{-1} of hMSCs (passage 2 and 3) was used for all studies. Cells were treated with the ionic product media for different time points (2, 4 and 7 days), and the cell viability was determined by MTT assay. MTT assays are a colorimetric method based on the conversion of 3-(4,5-dimethylthiazol-2-yl)-2,5-diphenyltetrazolium bromide (MTT) into formazan (Invitrogen, Molecular Probes™[NVAA1]). As a control, cells were cultured on plain α-MEM on tissue culture plate (TCP).

2.4 Ionic release products on hMSCs differentiation

To evaluate the effect of the BGs ionic products on the hMSCs differentiation, 5 x 10^4 cells.mL^{-1} were cultured in a flat-bottomed 24-well plate, and incubated for 24 h (37 °C and 5% CO_2), allowing cells to attach to the plate. Both conditions were used for the

cell culture: basal α-MEM or osteogenic medium (α-MEM supplemented with 100 μM L-ascorbic acid, 10 mM β-glycerophosphate and 10 nM dexamethasone). The culture media was changed twice a week.

The different sample groups were evaluated by colorimetric assay of ALP activity, histochemical evaluation by staining of Alizarin red S and immunofluorescence technique to detect type I collagen, osteocalcin (OSC) and osteopontin (OSP). The ALP activity was assessed using an Alkaline Phosphatase Assay Kit (Colorimetric, *Abcam*, UK, ab83369); values were normalised with respect to the total volume cell lysate and time and expressed as units per millilitre of cell lysate per minute. The absorbance of the reaction product was measured at 562 nm.

Immunofluorescence assay was performed after cells were fixed in 4% paraformaldehyde in PBS following 7, 14 and 21 days culture in basal and osteogenic medium. A permeability buffer for 30 min was applied followed by 1 % BSA in PBS for 5 min. Cells were then incubated overnight at 4 °C, with a rabbit IgG primary antibody (*Abcam*). The secondary antibody used for immunofluorescence was goat anti-rabbit IgH H&L conjugated with Alexa Fluor 455 (*Abcam*) The cell nuclei were stained with 4,6-Diamidino-2-Phenylindole, Dihydrochloride (DAPI, *Thermo Fisher Scientific*). Finally, to detect calcified tissue formation, cells were stained with 1% Alizarin Red S staining in PBS at pH 4.2.

3 Results and Discussion

3.1 Compositional analysis

The measured chemical compositions of Mn containing BGs final are shown in Table **1**. The variability of the final composition can be related to the use of diluted media for ICP analysis, filtration steps performed, losses during the glass dissolution, precipitation of species, amongst others [37]. Nonetheless, the presence of Mn on the BG samples was confirmed in two different compositions.

Table 1: Nominal composition and composition results of glasses based on the 58S composition and with Mn substitution for Ca, results obtained by the lithium metaborate method and ICP-OES (% mol).

	Nominal composition	**ICP-OES measured composition**

	(% mol)				(% mol)			
	SiO_2	P_2O_5	CaO	MnO	SiO_2	P_2O_5	CaO	MnO
0Mn	60.0	4.0	36.0	-	61.3 ± 0.9	3.2 ± 0.6	35.5 ± 0.9	-
2.5Mn	60.0	4.0	33.5	2.5	58.1 ± 1.6	4.0 ± 0.4	35.2 ± 2.0	2.7 ± 0.3
5Mn	60.0	4.0	31.0	5.0	59.0 ± 0.8	3.9 ± 0.4	32.7 ± 0.2	4.4 ± 0.5

3.2 Textural Properties

Nitrogen sorption analysis was performed to evaluate the glasses textural properties. Representative nitrogen adsorption/desorption isotherms are shown in Figure 1 (a), and the pore size distribution profile obtained from the nitrogen desorption curves are presented in Figure 1 (b). The obtained values for the specific surface area and pore size obtained by BET and BJH methods are shown in Table 2.

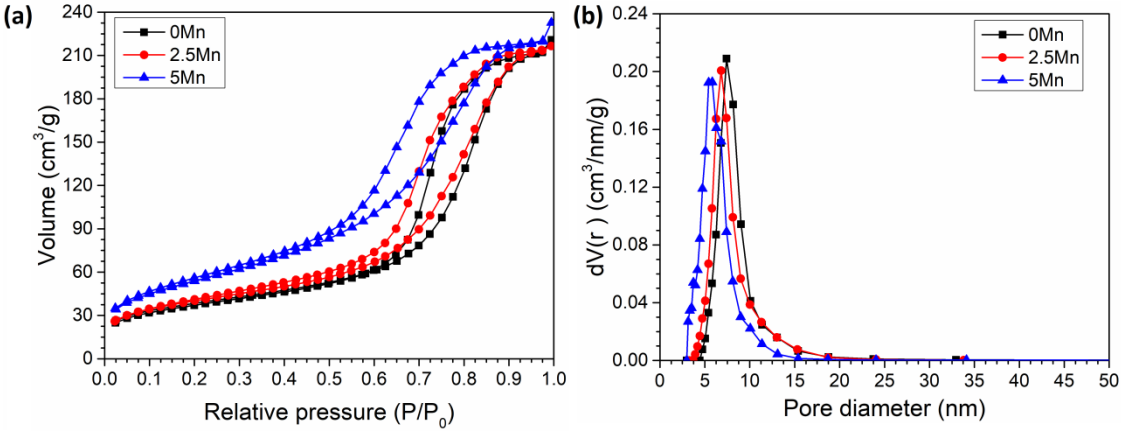

Figure 1: (a) Nitrogen sorption isotherms and (b) pore size distributions obtained using the BJH method applied to the desorption branches, for bioactive glass of the 58S composition (0Mn) and with MnO substitution for CaO at 2.5 mol% (2.5Mn) and 5 mol% (5Mn).

In all cases, Type IV isotherms with hysteresis cycle were identified, typical of materials containing pores in the mesoporous range (from 2 to 50 nm) [38]. Sol-gel derived materials typically present nanopores as a result of the removal of condensation by-products [39]. A narrow and monomodal pore size distribution was also observed for all samples (Figure 1 (b)). Glasses with high specific surface area (up to 130.0 ± 14.2 $m^2.g^{-1}$) were obtained and the pore diameter reduced from 7.6 ± 0.4 nm (0Mn) to 6.4 ± 0.2 nm for the glass containing higher Mn content (5Mn). The incorporation of additional ions

into the BG structure can affect the network orientation during the self-assembly reaction, consequently leading to potential structural defects and also to modification on the pore shape [40].

The pore diameter observed for all samples confirms that all materials exhibit a pore size in the mesoporous range. This is of great relevance for biomedical applications, as pores allow the adsorption of biological agents that could improve the body's response to the material [41]. Furthermore, BGs with high specific surface area containing pores in the mesoporous range could lead to improved dissolution rates and ion exchange processes, as well as act as nucleation sites for HCA formation, consequently inducing glass bioactivity.

Table 2: Textural properties obtained by nitrogen sorption evaluation for samples 0Mn, 2.5Mn and 5 Mn.

Samples	Specific surface area ($m^2.g^{-1}$)	Pore diameter (nm)
0Mn	124.0 ± 11.8	7.6 ± 0.4
2.5Mn	128.8 ± 15.2	6.6 ± 0.4
5Mn	130.0 ± 14.2	6.4 ± 0.2

3.3 Structural evaluation

FTIR spectra are presented in Figure 2 (a). Si-O bending can be observed between 450 and 470 cm^{-1}, assigned to glasses with Si-O-Si bonds with amorphous structures [42]. The symmetric (725 to 810 cm^{-1}) and asymmetric stretching (1000 to 1200 cm^{-1}) of Si-O bonds were also observed [43,44]. The absorbance with low relative intensity at around 965 cm^{-1} can be related to Si-O bonds containing a non-bridging oxygen (Si-O-NBO) [42]. The absorbance at around 1180 cm^{-1} can be related to stretching of P-O bonds, overlapping the absorbance related to Si-O bonds [43]. P-O bending bands, representative of orthophosphate groups (550 and 630 cm^{-1}) were present for the 58S glass (0Mn) [45]. These bands have previously been attributed, using solid state NMR, to phosphate-rich regions and hydroxyapatite nuclei that can be formed during sol-gel synthesis with excess water [46]. As Mn content increased, the relative intensity of the P-O bend bands decreased, which is likely to be due to the Mn charge balancing the phosphate groups and integrating the phosphate into the glass network.

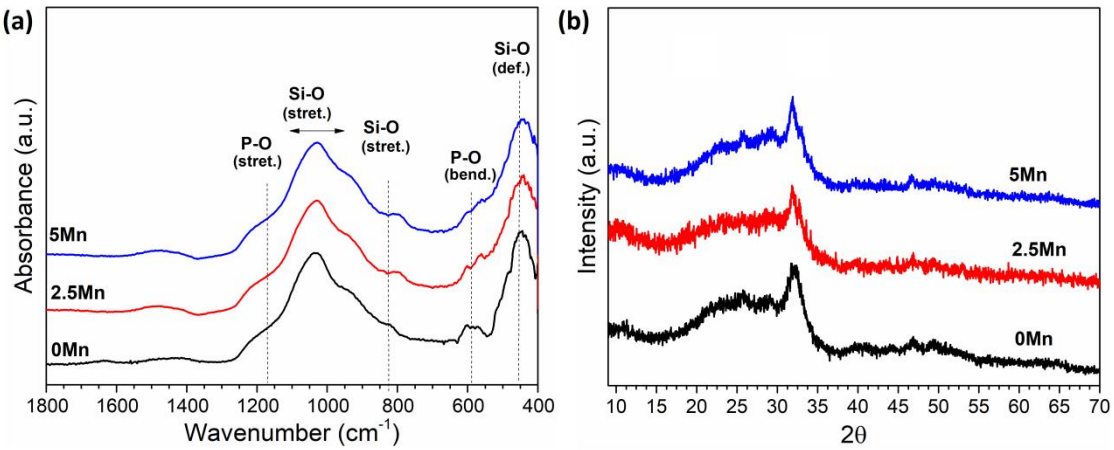

Figure 2: (a) FTIR spectra and (b) XRD patterns from bioactive glass of the 58S composition (0Mn) and with MnO substitution for CaO at 2.5 mol% (2.5Mn) and 5 mol% (5Mn).

The XRD patterns of BGs samples are shown in Figure 2 (b). Similar behaviour is observed in all samples, with a diffuse halo between 15 and 25 ° (2θ), characteristic of predominantly amorphous silica structures [47]. A less broad halo of greater intensity between 31 and 33 ° (2θ) can be assigned to the formation of the orthophosphate regions during synthesis, as reported in glasses previously obtained with similar composition [46]. These results indicate that the predominantly amorphous structure was maintained after Mn incorporation into the BGs.

The glass structure was further evaluated by XPS, and the survey scan spectra are presented in Figure 3. Auger and XPS photoemission lines typical of bioactive glass constituents were observed in all samples. Peak C 1s, related to the absorption of impurities of hydrocarbons by the glass surface, was used as a reference for calibration of the binding energy (BE) due to the charge effect of the samples, being adjusted to 285.0 eV.

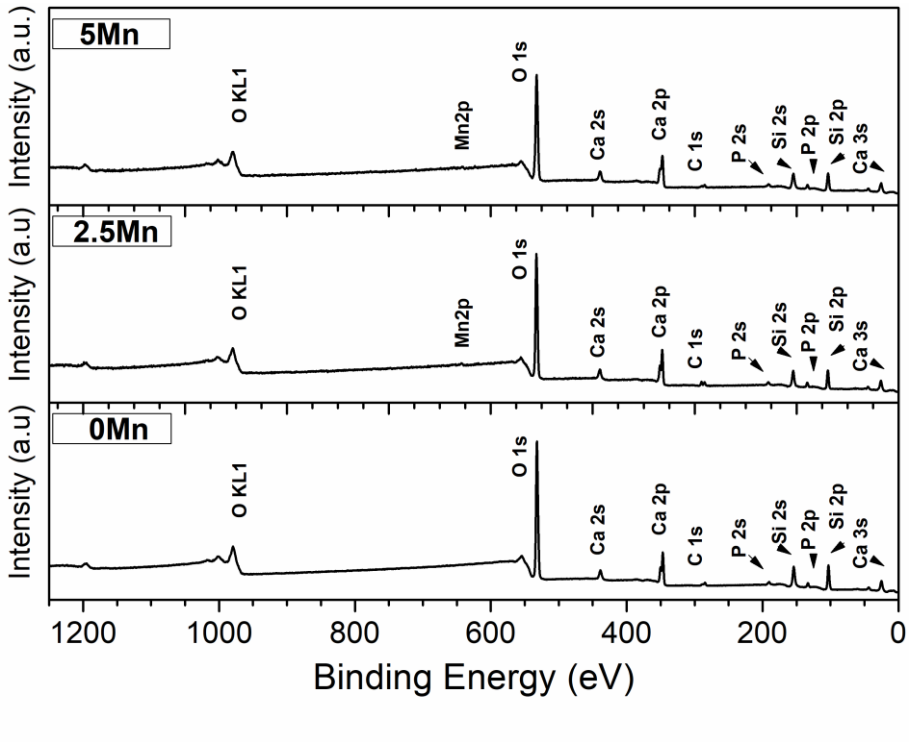

Figure 3: XPS survey scan spectra of bioactive glass of the 58S composition (0Mn) and with MnO substitution for CaO at 2.5 mol% (2.5Mn) and 5 mol% (5Mn).

High-resolution Si 2p XPS spectra are presented in Figure 4 (a), and broad bands with maxima at 103.5 eV, 103.6 eV and 103.6 eV were observed for 0Mn, 2.5Mn and 5Mn samples respectively, found in the typical range of silicate glasses [48].

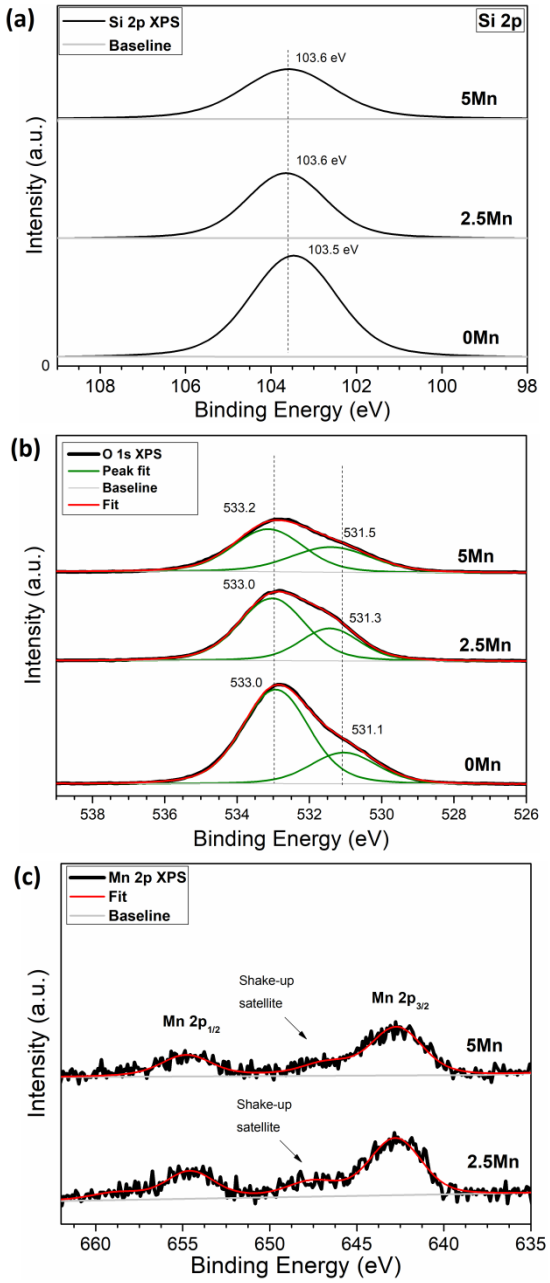

Figure 4: High-resolution XPS spectra (a) Si 2p, (b) O 1s and (c) Mn 2p for bioactive glass of the 58S composition (0Mn) and with MnO substitution for CaO at 2.5 mol% (2.5Mn) and 5 mol% (5Mn).

Figure 4 (b) shows the O 1s high-resolution XPS spectrum and two components with maximum binding energy at 531.1 eV and 533.0 eV can be observed for 0Mn, shifting to higher binding energy values when Mn was incorporated. The higher binding energy band observed after deconvolution can be assigned to the oxygen of silicates, whereas the band observed in lower values is related to the oxygen in phosphate groups [38]. Results indicate that calcium phosphate microdomains may be present in the glass structure, similar to the HCA environment, which may impart some heterogeneity to the material [38]. This agrees with the FTIR and XRD results and previous work that found

that the phosphorus was present mostly in the form of orthophosphates, and their charge is balanced by modified network cations, and only small amounts of Si-O-P bonds are observed [49].

Multiple peaks were observed on the high-resolution Mn 2p spectra (Figure 4 (c)), that can be attributed to the pairs from spin-orbit splitting (Mn $2p_{3/2}$ and Mn $2p_{1/2}$), with a maxima at 642.8 eV and 654.8 eV respectively. A satellite peak was also observed around 4 eV above the Mn $2p_{3/2}$ in both samples, assigned to the shake-up effect [50]. Manganese has six stable oxidation states, which may have significant division of multiplets and also overlapping binding energies, making them difficult to identify [51,52]. However, the observed peaks are within the range reported for manganese compounds [51,53,54]. In addition, the presence of the shake-up satellite structures is typical of Mn^{2+} species [55], indicating the majority presence of Mn^{2+} in the bioactive glass structure. In fact, previous works have shown that oxidation states such as +4 and +7 are unlikely in silicate systems and that this ion is normally present as Mn^{2+} in these structures, although Mn^{3+} can also be observed, shifting the Mn 2p bands to higher binding energy values [56–58]. The spectra also showed similar shape and Mn 2p position, indicating that even after incorporation of different Mn contents on the glass structure, the Mn chemical environment was maintained.

XPS evaluation showed that Mn is present in the bioactive glass network mainly as Mn^{2+} and no significant structural changes were observed due to the incorporation of this ion, as the O 1s and Si 2p spectra showed similar behaviour and binding energy, which is of interest to maintain the glass bioactive potential.

3.4 DMEM dissolution study

DMEM is often used as a cell culture environment, and the BG dissolution study in this medium is of great interest to correlate the material ionic dissolution profile to the results obtained during *in vitro* studies. The Si, Ca, P and Mn concentration in DMEM after soaking the glasses are presented in Figure 5.

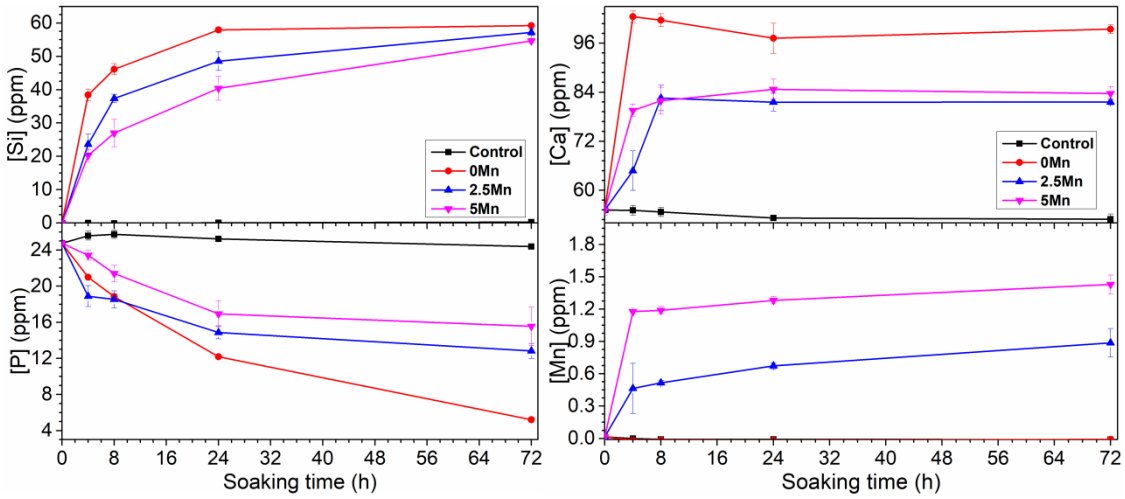

Figure 5: Si, P, Ca and Mn concentrations in DMEM after soaking bioactive glasses of the 58S composition (0Mn) and with MnO substitution for CaO at 2.5 mol% (2.5Mn) and 5 mol% (5Mn). Control is DMEM alone.

Si release for all samples was rapid for the first 24 h before stabilising. The release of Si decreased as Mn content increased. A maximum Si concentration of approximately 59 ppm was observed for 0Mn, a value that is within the reported range that shows stimulating effects on osteoblasts (0.1 to 100 ppm) [13,59]. The Ca release was also higher for 0Mn (Figure 5). The importance of Ca release in the bone mineralisation process is well established and can also induce osteoblast proliferation, consequently improving the therapeutic effect [59]. A reduction in the P concentration was observed, which is related to the migration of P to the material surface to form a calcium phosphate-rich region that may crystallise and form an HCA layer. The P concentration reduction was slower for Mn containing samples, indicating a slower calcium phosphate layer formation rate when Mn was present. HCA formation would be expected to be slower if Si and Ca dissolution is slower.

Mn was released rapidly during the first 4 hours, with Mn release increasing as Mn content increased, as expected due to the increased content of this ion in this sample, reaching a maximum of 1.4 ppm following 3 days of immersion in DMEM for 5Mn. Previous works report that osteoblast proliferation was inhibited when exposed to concentrations greater than 0.1 mM of $MnCl_2$ (~5.49 ppm Mn^{2+}), whereas the exposure of cells to lower concentrations of this ion improved the osteoblast proliferation and spreading [24]. Therefore, the Mn release profile should be properly adjusted in order to maintain the released concentration within the therapeutic range.

The BGs ability to release ions with therapeutic potential was confirmed by the DMEM dissolution study. The Mn incorporation reduced the glass dissolution rate, but a

controlled release of Si, Ca, P and Mn was observed on all samples. The amorphous structure obtained, with high surface area and predominance of NBO in its structure, affects the dissolution profile of the material, showing that the BG chemistry can be adjusted to release appropriate amounts of the different ions depending on the application.

3.5 Cytotoxicity analysis

Human mesenchymal stem cells (hMSCs) have an important role in tissue regeneration *in vivo* [60], being recruited by lesion sites, and can differentiate into different types of cells, such as bone, muscle, adipose cells, etc. [61]. Bone marrow derived hMSCs are extensively used for cell therapies and different strategies in tissue engineering. Here, cell viability was evaluated after exposure of hMSCs to the dissolution products of the BGs (Figure 6). Materials are considered cytotoxic when cell viability is reduced by more than 30% (ISO 10993-5) [12]. No cytotoxic effect was observed when hMSCs were exposed to the dissolution products of any of the samples, prepared as 1.5 mg of glass per mL of DMEM for 4 h, for up to seven days exposure of the cells to the conditioned media. An increase in the mitochondrial activity was observed after four days exposure to the dissolution products of all samples when compared to the control, although no significant statistical differences were observed between 0Mn and the Mn-containing groups (2.5Mn and 5Mn). These results indicate that the dissolution products of the BG samples did not significantly alter the mitochondrial metabolic activity, and Mn-containing samples are not cytotoxic under the conditions evaluated.

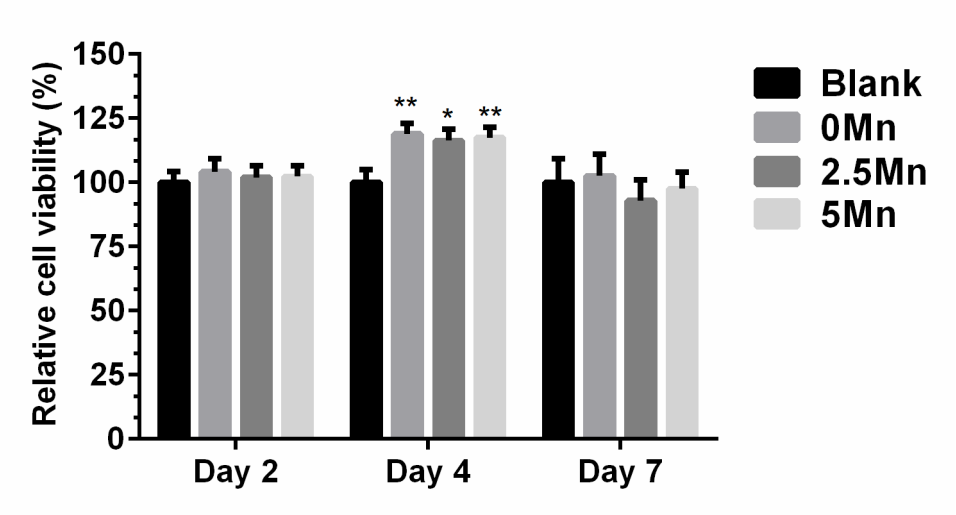

Figure 6: Cell viability determined by MTT in hMSCs exposed to dissolution media (1.5 mg glass per mL of DMEM) from glasses of the 58S composition (0Mn) and with MnO substitution for CaO at 2.5 mol% (2.5Mn) and 5 mol% (5Mn). Control was DMEM. Mean cell viability normalized by the mean viability of the control group. $p < 0.05$ (*) or $p < 0.01$

(**) in relation to the control as determined by One-way ANOVA method followed by Tukey post-hoc test, n = ?.

3.6 Evaluation of hMSCs differentiation markers

As osteoblasts differentiate from hMSCs, they express various proteins, growth factors, and transcription factor, which exhibit different expression patterns over time [62]. Usually, after osteoblastic cells are plated in osteogenic medium, three differentiation stages can be observed: proliferation, matrix production/maturation and mineralisation. The proliferative phase involves the expression of histone and cell cycle genes and is followed by the expression of genes and proteins such as collagen type I and ALP activity, associated with bone matrix formation. In the final stage, proteins associated with mineralisation such as osteopontin, osteocalcin and bone sialoprotein are expressed at the highest levels [62].

To evaluate the effect of BG dissolution products in osteogenic differentiation, different bone formation markers were investigated. Figure 7 shows the ALP activity of hMSCs exposed to the dissolution products of 0Mn, 2.5Mn and 5Mn BGs, following 7, 14 and 21 days culture (ions in basal medium), and the control group (basal medium). ALP is an early stage marker of osteoblastic differentiation and is essential for degradation pyrophosphate to release phosphates for mineralisation [8]. Previous studies report that ALP production by newborn rat calvaria-derived osteoblastic cells was enhanced by the BGs dissolution products, but its activity reduced when the cells became confluent and initiated mineralisation (not observed in this work) [63]. The time at which the reduction of the ALP due to the mineralisation onset occurred was expected to be slower in basal medium (without osteogenic supplements), than in the osteogenic condition. However, no decrease was observed, instead the ALP expression continued to increase over the three weeks, indicating the progression of the cellular differentiation process, being stimulated by the presence of the BGs ionic products. The highest ALP expression was observed for the Mn-containing samples, indicating Mn may influence the hMSC differentiation process.

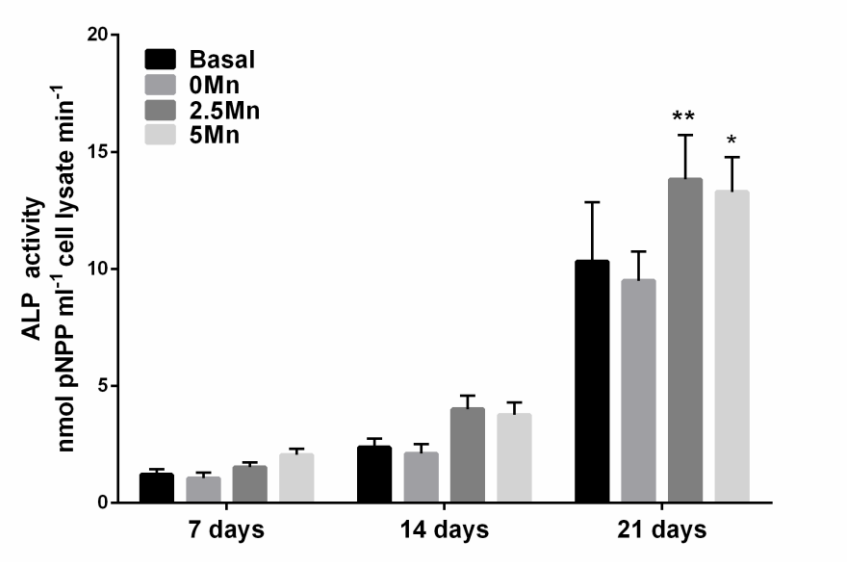

Figure 7: Alkaline phosphatase (ALP) activity of hMSCs after 7, 14 and 21 days of exposure to the dissolution products of bioactive glasses of 58S composition (0Mn) and with MnO substitution for CaO at 2.5 mol% (2.5Mn) and 5 mol% (5Mn). (*p<0.05 and **p<0.01 related to the basal control, Two-way ANOVA and Tukey multiple comparison tests, n = ?).

Osteogenic differentiation markers, such as type I collagen, OSC and OSP, were also evaluated using immunofluorescence (Figure 8). Cell nuclei are represented in blue (DAPI dye), and the collagen type I, OSP and OSC protein expression green (Figure 8). Type I collagen is a marker associated with ECM formation [64] and is commonly seen in initial stage osteoblast differentiation. During osteoblast differentiation, the expression of type I collagen is relatively high and can also be produced intrinsically by cells, with subsequent reduction according to the progression of the differentiation and mineralisation stages [65]. Here, high collagen type I expression was observed in both osteogenic and basal media, with no significant differences between the cells exposed to the ionic products of different samples. Results show that the ECM can form even without osteogenic supplements, as a high collagen type I expression was also observed in basal medium.

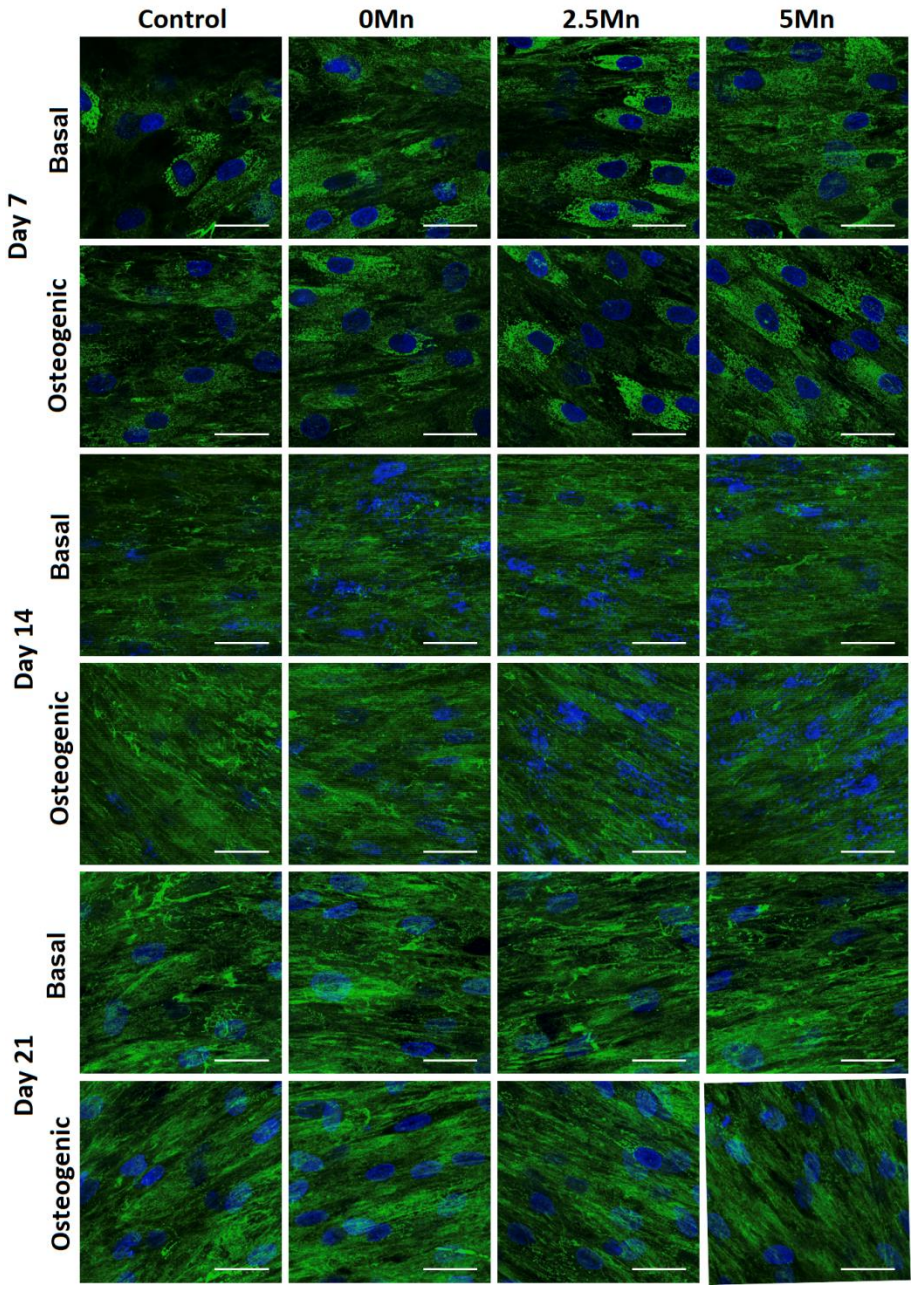

Figure 8: Fluorescence images of hMSCs, DAPI dyes (blue) and collagen type I (green), following exposure to the dissolution products of bioactive glasses of the 58S composition (0Mn) and with MnO substitution for CaO at 2.5 mol% (2.5Mn) and 5 mol% (5Mn), presenting the type I collagen expression in basal and osteogenic media after 7, 14 and 21 days. Control is the media without the glass dissolution products. Scale bar is 50 µm.

OSP is an osteogenic marker that regulates mineral nodule formation and leads to osteogenesis. Its expression is therefore usually related to the mineralisation ability of the cells [8]. Non-collagenous proteins such as OSP control HCA nucleation, growth, shape and size of the HCA crystals and also plays a role on the organic (collagen) and inorganic (HCA) fraction binding in the bone tissue [66]. OSP expression is usually

observed prior to the OSC expression in the osteogenic differentiation process, but both are expressed only by completely differentiated osteoblasts [65].

OSP expression of hMSCs in both basal and osteogenic media after 7, 14 and 21 days exposure to the BGs ionic products is presented in Figure 9. After 7 days, no OSP expression was observed. It was observed in osteogenic medium after 14 days exposure, and after 21 days the OSP expression was present in both osteogenic and basal media for all samples. ALP and type I collagen are usually expressed during the initial differentiation stages but are replaced by the OSP expression overtime, in agreement to the results observed in this work. Figure 9 shows osteogenic medium was not needed for expression of the OSP marker, as expression was observed in the Mn containing samples after three weeks in culture, with more OSP expressed for the 5Mn sample. The results were not clear cut however, as while little OSP was observed in the cells exposed to the 58S dissolution products, some OSP was observed for the basal medium culture (without dissolution products). Osteogenic media did accelerate OSP expression (expression seen at day 14).

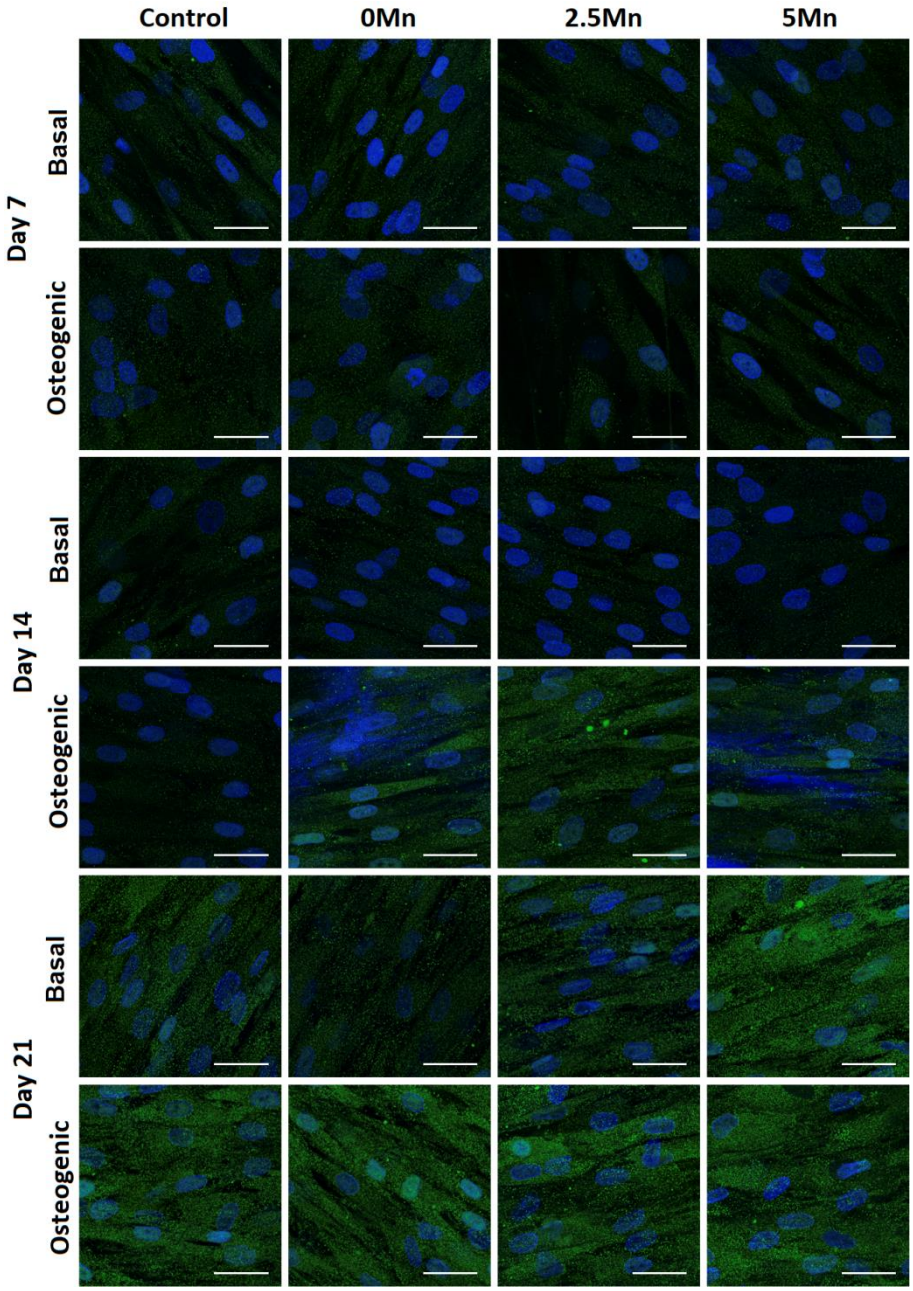

Figure 9: Fluorescence images of hMSCs, DAPI dyes (blue) and osteopontin (green), following exposure to the dissolution products of bioactive glasses of the 58S composition (0Mn) and with MnO substitution for CaO at 2.5 mol% (2.5Mn) and 5 mol% (5Mn), presenting the osteopontin expression in basal and osteogenic medium after 7, 14 and 21 days. Controls are DMEM without dissolution products. Scale bar is 50 µm.

In the hierarchical sequence of events that occur during hMSC differentiation down the osteoblast lineage, type I collagen biosynthesis and ALP activity are followed by OSP expression, bone sialoprotein deposition and subsequently OSC synthesis [67], an ECM non-collagenous protein, considered the most specific marker for mature osteoblasts, characteristic of the final differentiation stages [68]. Figure 10 shows high OSC expression after 21 days of hMSCs exposure to the BGs ionic products, both in basal and osteogenic medium, suggesting the development of a typical mature osteoblast

phenotype due to the glass ionic release. Cells exposed to the Mn-containing dissolution products presented higher OSC expression intensity when compared to control and 0Mn, indicating that the presence of Mn was conducive to the formation of mature osteoblasts and bone mineralisation processes.

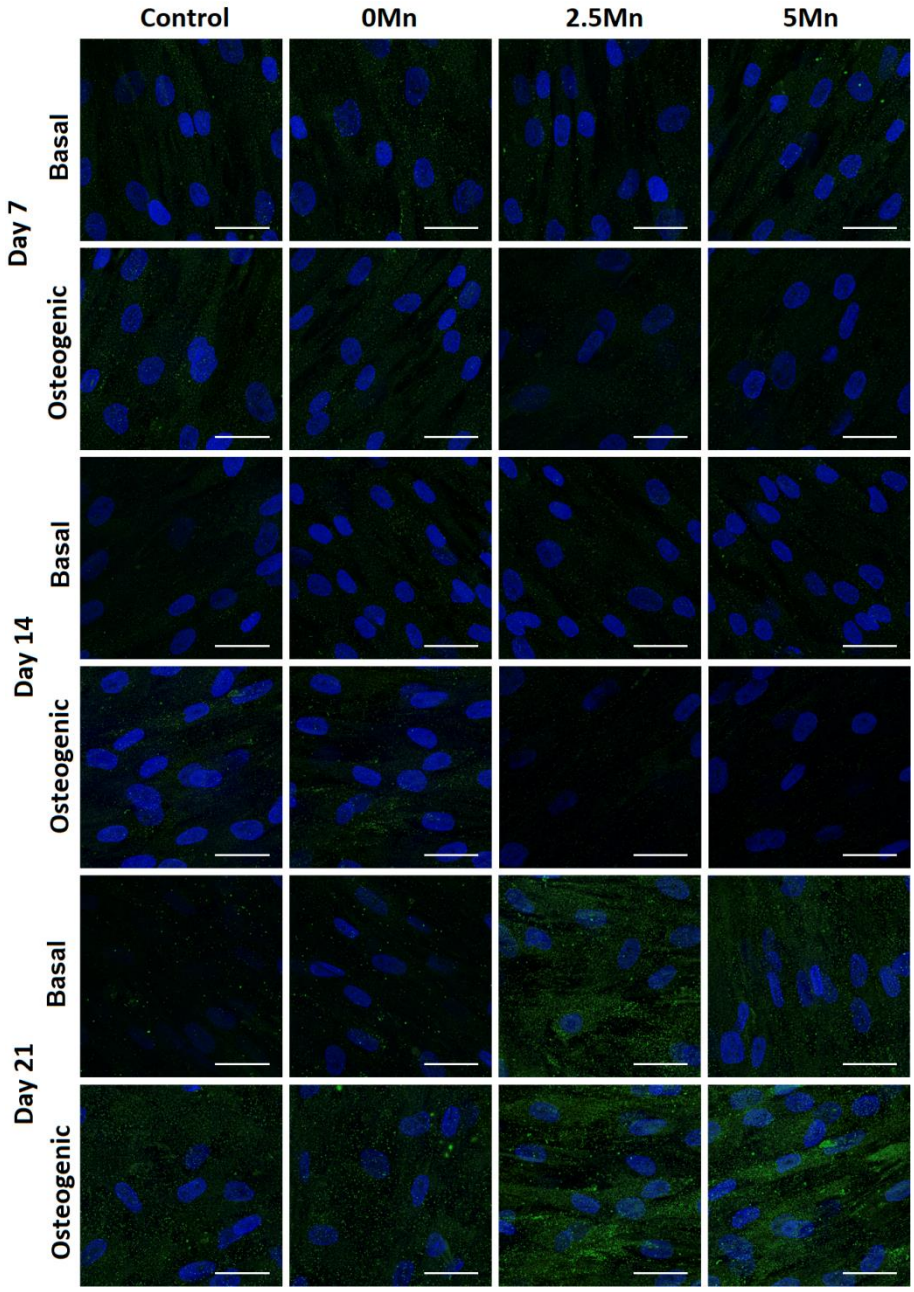

Figure 10: Fluorescence images of hMSCs, DAPI dyes (blue) and osteocalcin (green), following exposure to the dissolution products of bioactive glasses of the 58S composition (0Mn) and with MnO substitution for CaO at 2.5 mol% (2.5Mn) and 5 mol% (5Mn), presenting osteocalcin expression in basal and osteogenic media after 7, 14 and 21 days. Scale bar is 50 µm.

hMSCs were stained using alizarin red S to verify the presence of calcium deposits that are formed once the bone mineralisation process is completed [8] (Figure 11). No

calcium deposits were observed after 7 days, in accordance with previous results that show that the differentiation process was still in the initial phase. However, after 14 days, calcium nodules were observed, with higher intensity for the cultures in osteogenic medium, in which the presence of osteogenic supplements may have accelerated the mineralisation process. After 21 days, calcium nodules were observed in basal medium cultured groups, with the dissolution ions producing more mineralisation compared to basal control, indicating the influence of the dissolution product on the hMSC differentiation and mineralisation processes. In osteogenic medium, calcium deposit formation was higher when hMSCs were exposed to the dissolution products of the BGs compared to control in osteogenic medium. Results are in agreement with previously observed for OSC and OSP expression, associated with mineralisation, that showed higher expression after 14 days in osteogenic medium and 21 days when in basal medium. This study also confirms that osteogenic supplements are not necessary for hMSCs differentiation and mineralisation process, but can accelerate it. This process can also be stimulated by the BGs ionic products, but the synergistic effect between the glass dissolution product and the osteogenic supplements may favor the process.

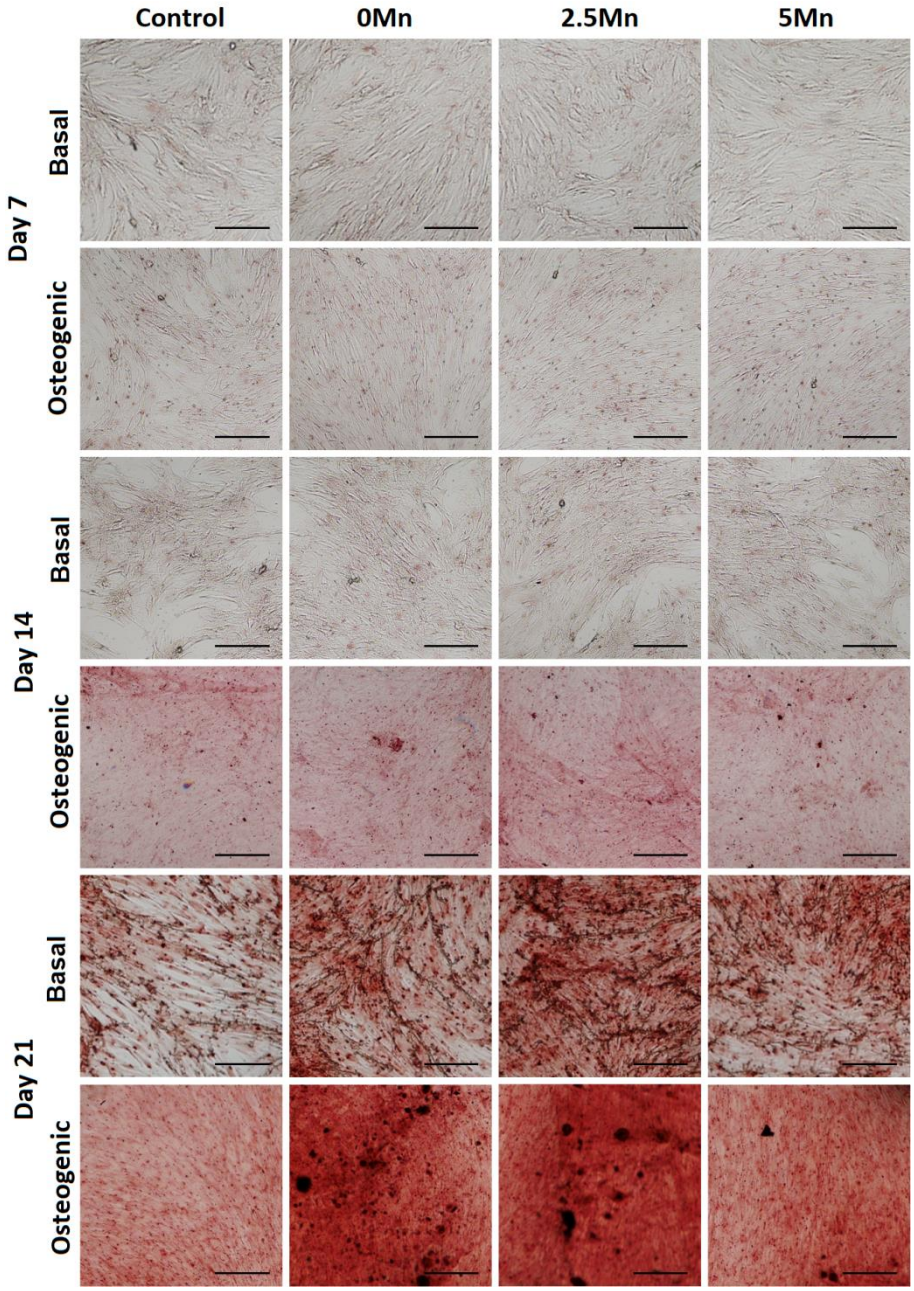

Figure 11: Matrix mineralisation of hMSCs exposed to the dissolution products of bioactive glasses, of 58S composition (0Mn) and with MnO substitution for CaO at 2.5 mol% (2.5Mn) and 5 mol% (5Mn), in basal and osteogenic media after 7, 14 and 21 days. Cells were stained with alizarin red S for calcium deposits visualization. Scale bar is 100 µm.

This study showed that the BGs dissolution products were able to stimulate all hMSCs differentiation stages and subsequent mineralisation in 21 days culture analysis. The initial differentiation process was demonstrated by the ALP and type I collagen expression, observed in all culture conditions, followed by OSP (mineral nodules formation regulator) and OSC (development of mature osteoblasts indicator). Calcium deposits were also observed, and indicative of the mineralisation process. Results showed that the BG dissolution products stimulated hMSC osteogenic differentiation in

basal medium (with no osteogenic supplements), and Mn-containing dissolution product can influence the formation of mature osteoblasts. Therefore, Mn incorporation features as a potential strategy to stimulate bone healing and improve bone tissue repair.

4 Conclusions

Sol-gel-derived bioactive glass in the SiO_2-CaO-P_2O_5-MnO system, containing up to 4.4 ± 0.5 mol% Mn were obtained with high specific surface area and inherent nanoporosity. Structural evaluation showed that manganese nitrate is an effective precursor for Mn incorporation, and no significant changes in the glass network were observed when compared to the 58S (SiO_2-CaO-P_2O_5) system. A predominantly amorphous structure was obtained, favourable to maintain the glass bioactivity. The presence of Mn^{2+} species and a controlled ion release in DMEM was also observed. No cytotoxic effect was observed when hMSCs were exposed to the glass dissolution products. The dissolution products from the Mn containing glasses stimulated hMSCs osteogenic differentiation stages and subsequent mineralisation, which this was not clear for the 58S Mn-free composition. The effect of Mn on the differentiation and mineralisation processes was observed mainly by the OSC marker, in which a greater expression was observed when this ion was present, indicating that the Mn incorporation is a potential strategy to obtain superior materials for bone regeneration.

Acknowledgements

The authors acknowledge financial support from CNPq, CAPES and FAPEMIG/Brazil and to the Advanced Photoelectron Spectroscopy Laboratory (APSL – Department of Materials - Imperial College London) for XPS analysis.

Conflict of interest

The authors declare that there is no personal or financial conflict of interests in the current paper.

5 References

[1] L.L. Hench, R.J. Splinter, W.C. Allen, T.K. Greenlee, Bonding mechanisms at the interface of ceramic prosthetic materials, J. Biomed. Mater. Res. 5 (1971) 117–141. doi:10.1002/jbm.820050611.

[2] F. Baino, Bioactive glasses – When glass science and technology meet regenerative medicine, Ceram. Int. 44 (2018) 14953–14966.

doi:10.1016/j.ceramint.2018.05.180.

[3] J.R. Jones, D.S. Brauer, L. Hupa, D.C. Greenspan, Bioglass and Bioactive Glasses and Their Impact on Healthcare, Int. J. Appl. Glas. Sci. 7 (2016) 423–434. doi:10.1111/ijag.12252.

[4] I.D. Xynos, A.J. Edgar, L.D.K. Buttery, L.L. Hench, J.M. Polak, Gene-expression profiling of human osteoblasts following treatment with the ionic products of Bioglass 45S5 dissolution, J. Biomed. Mater. Res. 55 (2001) 151–157. doi:10.1002/1097-4636(200105)55:2<151::AID-JBM1001>3.0.CO;2-D.

[5] M. Bosetti, M. Cannas, The effect of bioactive glasses on bone marrow stromal cells differentiation, Biomaterials. 26 (2005) 3873–3879. doi:10.1016/j.biomaterials.2004.09.059.

[6] G.C. Reilly, S. Radin, A.T. Chen, P. Ducheyne, Differential alkaline phosphatase responses of rat and human bone marrow derived mesenchymal stem cells to 45S5 bioactive glass, Biomaterials. 28 (2007) 4091–4097. doi:10.1016/j.biomaterials.2007.05.038.

[7] R.C. Bielby, D. Phil, R.S. Pryce, M. Phys, D. Ph, L.L. Hench, B. Sc, D. Ph, J.M. Polak, D. Sc, Enhanced Derivation of Osteogenic Cells from Murine Embryonic Stem Cells after Treatment with Ionic Dissolution Products of 58S Bioactive Sol – Gel Glass, Tissue Eng. 11 (2005).

[8] A.B. Houreh, S. Labbaf, H.-K. Ting, F. Ejeian, J.R. Jones, M.-H.N. Esfahani, Influence of calcium and phosphorus release from bioactive glasses on viability and differentiation of dental pulp stem cells, J. Mater. Sci. (2017). doi:10.1007/s10853-017-0946-4.

[9] J.R. Jones, Review of bioactive glass: From Hench to hybrids, Acta Biomater. 9 (2013) 4457–4486. doi:10.1016/j.actbio.2012.08.023.

[10] F. Baino, E. Fiume, M. Miola, E. Verné, Bioactive sol-gel glasses: Processing, properties, and applications, Int. J. Appl. Ceram. Technol. 15 (2018) 841–860. doi:10.1111/ijac.12873.

[11] P. Naruphontjirakul, S.L. Greasley, S. Chen, A.E. Porter, J.R. Jones, Monodispersed strontium containing bioactive glass nanoparticles and MC3T3-E1 cellular response, Biomed. Glas. 2 (2016) 72–81. doi:10.1515/bglass-2016-

0009.

[12] P. Naruphontjirakul, A.E. Porter, J.R. Jones, In vitro osteogenesis by intracellular uptake of strontium containing bioactive glass nanoparticles, Acta Biomater. (2017). doi:10.1016/j.actbio.2017.11.008.

[13] E. Gentleman, Y.C. Fredholm, G. Jell, N. Lotfibakhshaiesh, M.D. O'Donnell, R.G. Hill, M.M. Stevens, The effects of strontium-substituted bioactive glasses on osteoblasts and osteoclasts in vitro, Biomaterials. 31 (2010) 3949–3956. doi:10.1016/j.biomaterials.2010.01.121.

[14] M.E. Santocildes-romero, A. Crawford, P. V Hatton, R.L. Goodchild, I.M. Reaney, C.A. Miller, The osteogenic response of mesenchymal stromal cells to strontium-substituted bioactive glasses, J. Tissue Eng. Regen. Med. 9 (2015) 619–631. doi:10.1002/term.2003.

[15] F. Yang, D. Yang, J. Tu, Q. Zheng, L. Cai, L. Wang, Strontium Enhances Osteogenic Differentiation of Mesenchymal Stem Cells and In Vivo Bone Formation by Activating Wnt / Catenin, Stem Cells. 29 (2011) 981–991. doi:10.1002/stem.646.

[16] L. Cabrini, M.P. Lo, A.A. Gorustovich, T. Steimetz, M.P. Bfdq, Osteoconductivity of strontium-doped bioactive glass particles : A histomorphometric study in rats, J. Biomed. Mater. Res. Part A. 92A (2009) 232–237. doi:10.1002/jbm.a.32355.

[17] H. Autefage, E. Gentleman, E. Littmann, M.A.B. Hedegaard, T. Von Erlach, M. O'Donnell, F.R. Burden, D.A. Winkler, M.M. Stevens, Sparse feature selection methods identify unexpected global cellular response to strontium-containing materials, PNAS. 112 (2015) 4280–4285. doi:10.1073/pnas.1419799112.

[18] P. Naruphontjirakul, O. Tsigkou, S. Li, A.E. Porter, J.R. Jones, Human mesenchymal stem cells differentiate into an osteogenic lineage in presence of strontium containing bioactive glass nanoparticles, Acta Biomater. (2019). doi:10.1016/j.actbio.2019.03.038.

[19] E.G. Pires, R.F. Bonan, Í.M. Rocha, I.M.F. Gonçalves, J.R. de Souza, L.H.V. Gonzales, J.V.J. da Silva Junior, D.E. da C. Perez, P.C.B. Tavares, S.M. da Silva, R.P. Alves-Balvedi, L.R. Goulart, E.S. de Medeiros, L.R. Castellano, P.R.F. Bonan, Silver-doped 58S bioactive glass as an anti-Leishmania agent, Int. J. Appl. Glas. Sci. 1 (2017) 52–61. doi:10.1111/ijag.12285.

[20] A. Rahimnejad Yazdi, L. Torkan, W. Stone, M.R. Towler, The impact of gallium content on degradation, bioactivity, and antibacterial potency of zinc borate bioactive glass, J. Biomed. Mater. Res. Part B Appl. Biomater. (2017) 1–10. doi:10.1002/jbm.b.33856.

[21] B.R. Barrioni, A.G.S. de Laia, T.M. Valverde, T.M. da M. Martins, M.V. Caliari, M.A. de Sá, A.M. de Goes, M. de M. Pereira, Evaluation of in vitro and in vivo biocompatibility and structure of cobalt-releasing sol-gel bioactive glass, Ceram. Int. 44 (2018) 20337–20347. doi:10.1016/j.ceramint.2018.08.022.

[22] M. Azevedo, G. Jell, M. O'Donnell, R. Law, R. Hill, M. Stevens, Synthesis and characterization of hypoxia-mimicking bioactive glasses for skeletal regeneration, J. Mater. Chem. 20 (2010) 8854–8864. doi:10.1039/c0jm01111h.

[23] L.B. Romero-Sánchez, M. Marí-Beffa, P. Carrillo, M.Á. Medina, A. Díaz-Cuenca, Copper-containing mesoporous bioactive glass promotes angiogenesis in an in vivo zebrafish model, Acta Biomater. (2018). doi:10.1016/j.actbio.2017.12.032.

[24] F. Lüthen, U. Bulnheim, P.D. Müller, J. Rychly, H. Jesswein, J.G.B. Nebe, Influence of manganese ions on cellular behavior of human osteoblasts in vitro, Biomol. Eng. 24 (2007) 531–536. doi:10.1016/j.bioeng.2007.08.003.

[25] M. Miola, C.V. Brovarone, G. Maina, F. Rossi, L. Bergandi, D. Ghigo, S. Saracino, M. Maggiora, R.A. Canuto, G. Muzio, E. Vernè, In vitro study of manganese-doped bioactive glasses for bone regeneration, Mater. Sci. Eng. C. 38 (2014) 107–118. doi:10.1016/j.msec.2014.01.045.

[26] Y.J. Bae, M.H. Kim, Manganese supplementation improves mineral density of the spine and femur and serum osteocalcin in rats, Biol. Trace Elem. Res. 124 (2008) 28–34. doi:10.1007/s12011-008-8119-6.

[27] W. Fujitani, Y. Hamada, N. Kawaguchi, S. Mori, K. Daito, A. Uchinaka, T. Matsumoto, Y. Kojima, M. Daito, T. Nakano, N. Matsuura, Synthesis of Hydroxyapatite Containing Manganese and Its Evaluation of Biocompatibility, Nano Biomed. 2 (2010) 37–46. doi:10.11344/nano.2.37.

[28] P.M.C. Torres, S.I. Vieira, a. R. Cerqueira, S. Pina, O. a B. Da Cruz Silva, J.C.C. Abrantes, J.M.F. Ferreira, Effects of Mn-doping on the structure and biological properties of β-tricalcium phosphate, J. Inorg. Biochem. 136 (2014) 57–66. doi:10.1016/j.jinorgbio.2014.03.013.

[29] L. Yu, Y. Tian, Y. Qiao, X. Liu, Mn-containing titanium surface with favorable osteogenic and antimicrobial functions synthesized by PIII&D, Colloids Surfaces B Biointerfaces. 152 (2017) 376–384. doi:10.1016/j.colsurfb.2017.01.047.

[30] N. Sharma, S. Jandaik, S. Kumar, M. Chitkara, I.S. Sandhu, Synthesis, characterisation and antimicrobial activity of manganese- and iron-doped zinc oxide nanoparticles, J. Exp. Nanosci. 11 (2016) 54–71. doi:10.1080/17458080.2015.1025302.

[31] Q. Nawaz, M. Atiq, U. Rehman, A. Burkovski, J. Schmidt, A.M. Beltrán, A. Shahid, N.K. Alber, W. Peukert, A.R. Boccaccini, Synthesis and characterization of manganese containing mesoporous bioactive glass nanoparticles for biomedical applications, J. Mater. Sci. Mater. Med. 5 (2018). doi:10.1007/s10856-018-6070-4.

[32] B.R. Barrioni, A.C. Oliveira, M. de Fátima Leite, M. de Magalhães Pereira, Sol–gel-derived manganese-releasing bioactive glass as a therapeutic approach for bone tissue engineering, J. Mater. Sci. 52 (2017) 8904–8927. doi:10.1007/s10853-017-0944-6.

[33] R. Li, A.E. Clark, L.L. Hench, An investigation of bioactive glass powders by sol-gel processing., J. Appl. Biomater. 2 (1991) 231–239. doi:10.1002/jab.770020403.

[34] S. Brunauer, P.H. Emmett, E. Teller, Gases in Multimolecular Layers, J. Am. Chem. Soc. 60 (1938) 309–319. doi:10.1021/ja01269a023.

[35] E.P. Barrett, L.G. Joyner, P.P. Halenda, The Determination of Pore Volume and Area Distributions in Porous Substances. I. Computations from Nitrogen Isotherms, J. Am. Chem. Soc. 73 (1951) 373–380. doi:10.1021/ja01145a126.

[36] A.L.B. Maçon, T.B. Kim, E.M. Valliant, K. Goetschius, R.K. Brow, D.E. Day, A. Hoppe, A.R. Boccaccini, I.Y. Kim, C. Ohtsuki, T. Kokubo, A. Osaka, M. Vallet-Regí, D. Arcos, L. Fraile, A.J. Salinas, A. V Teixeira, Y. Vueva, R.M. Almeida, M. Miola, C. Vitale-Brovarone, E. Verné, W. Höland, J.R. Jones, A unified in vitro evaluation for apatite-forming ability of bioactive glasses and their variants, J. Mater. Sci. Mater. Med. 26 (2015) 115. doi:10.1007/s10856-015-5403-9.

[37] A.A.R. de Oliveira, D.A. de Souza, L.L.S. Dias, S.M. de Carvalho, H.S. Mansur, M. de Magalhães Pereira, Synthesis, characterization and cytocompatibility of

spherical bioactive glass nanoparticles for potential hard tissue engineering applications, Biomed. Mater. 8 (2013) 025011. doi:10.1088/1748-6041/8/2/025011.

[38] J. Perez-Pariente, F. Balas, M. Vallet-Regi, Surface and chemical study of SiO2.P2O5.CaO.(MgO) bioactive glasses, Chem. Mater. 12 (2000) 750–755. doi:10.1021/cm9911114.

[39] S. Lin, C. Ionescu, K.J. Pike, M.E. Smith, J.R. Jones, Nanostructure evolution and calcium distribution in sol-gel derived bioactive glass, J. Mater. Chem. 19 (2009) 1276–1282. doi:10.1039/b814292k.

[40] I. Atkinson, E.M. Anghel, L. Predoana, O.C. Mocioiu, L. Jecu, I. Raut, C. Munteanu, D. Culita, M. Zaharescu, Influence of ZnO addition on the structural, in vitro behavior and antimicrobial activity of sol–gel derived CaO–P2O5–SiO2 bioactive glasses, Ceram. Int. 42 (2016) 3033–3045. doi:10.1016/j.ceramint.2015.10.090.

[41] P.N. Gunawidjaja, R. Mathew, a. Y.H. Lo, I. Izquierdo-Barba, a. Garcia, D. Arcos, M. Vallet-Regi, M. Eden, Local structures of mesoporous bioactive glasses and their surface alterations in vitro: inferences from solid-state nuclear magnetic resonance, Philos. Trans. R. Soc. A Math. Phys. Eng. Sci. 370 (2012) 1376–1399. doi:10.1098/rsta.2011.0257.

[42] A.M. El-Kady, A.F. Ali, Fabrication and characterization of ZnO modified bioactive glass nanoparticles, Ceram. Int. 38 (2012) 1195–1204. doi:10.1016/j.ceramint.2011.07.069.

[43] C.D.F. Moreira, S.M. Carvalho, H.S. Mansur, M.M. Pereira, Thermogelling chitosan–collagen–bioactive glass nanoparticle hybrids as potential injectable systems for tissue engineering, Mater. Sci. Eng. C. 58 (2016) 1207–1216. doi:10.1016/j.msec.2015.09.075.

[44] G. Lusvardi, G. Malavasi, L. Menabue, S. Shruti, Gallium-containing phosphosilicate glasses: Functionalization and in-vitro bioactivity, Mater. Sci. Eng. C. 33 (2013) 3190–3196. doi:10.1016/j.msec.2013.03.046.

[45] C. Paluszkiewicz, A. Ślósarczyk, D. Pijocha, M. Sitarz, M. Bućko, A. Zima, A. Chróścicka, M. Lewandowska-Szumieł, Synthesis, structural properties and thermal stability of Mn-doped hydroxyapatite, J. Mol. Struct. 976 (2010) 301–309.

doi:10.1016/j.molstruc.2010.04.001.

[46] H.-K. Ting, S. Page, G. Poologasundarampillai, S. Chen, J. V. Hanna, J.R. Jones, Phosphate content affects structure and bioactivity of sol-gel silicate bioactive glasses, Int. J. Appl. Glas. Sci. (2017). doi:10.1111/ijag.12322.

[47] a. Saboori, M. Rabiee, F. Moztarzadeh, M. Sheikhi, M. Tahriri, M. Karimi, Synthesis, characterization and in vitro bioactivity of sol-gel-derived SiO2-CaO-P2O5-MgO bioglass, Mater. Sci. Eng. C. 29 (2009) 335–340. doi:10.1016/j.msec.2008.07.004.

[48] A.M. Toufiq, F. Wang, Q. Javed, Y. Li, Influence of SiO2 on the structure-controlled synthesis and magnetic properties of prismatic MnO2 nanorods., Nanotechnology. 24 (2013) 415703. doi:10.1088/0957-4484/24/41/415703.

[49] F. Fayon, C. Duée, T. Poumeyrol, M. Allix, D. Massiot, Evidence of nanometric-sized phosphate clusters in bioactive glasses as revealed by solid-state 31P NMR, J. Phys. Chem. C. 117 (2013) 2283–2288. doi:10.1021/jp312263j.

[50] R. Gostynski, J. Conradie, E. Erasmus, Significance of the electron-density of molecular fragments on the properties of manganese(iii) β-diketonato complexes: an XPS and DFT study, RSC Adv. 7 (2017) 27718–27728. doi:10.1039/C7RA04921H.

[51] M.C. Biesinger, B.P. Payne, A.P. Grosvenor, L.W.M. Lau, A.R. Gerson, R.S.C. Smart, Resolving surface chemical states in XPS analysis of first row transition metals, oxides and hydroxides: Cr, Mn, Fe, Co and Ni, Appl. Surf. Sci. 257 (2011) 2717–2730. doi:10.1016/j.apsusc.2010.10.051.

[52] J.M. Cerrato, M.F. Hochella, W.R. Knocke, A.M. Dietrich, T.F. Cromer, Use of XPS to identify the oxidation state of Mn in solid surfaces of filtration media oxide samples from drinking water treatment plants, Environ. Sci. Technol. 44 (2010) 5881–5886. doi:10.1021/es100547q.

[53] H.W. Nesbitt, D. Banerjee, Interpretation of XPS Mn(2p) spectra of Mn oxyhydroxides and constraints on the mechanism of MnO2 precipitation, Am. Mineral. 83 (1998) 305–315. doi:10.2138/am-1998-3-414.

[54] C. Poinsignon, G. Berthomé, B. Prélot, F. Thomas, F. Villiéras, Manganese Dioxides Surface Properties Studied by XPS and Gas Adsorption, J. Electrochem.

Soc. 151 (2004) A1611–A1616. doi:10.1149/1.1789411.

[55] O.A. Bulavchenko, Z.S. Vinokurov, T.N. Afonasenko, P.G. Tsyrul'nikov, S. V Tsybulya, A.A. Saraev, V. V Kaichev, Reduction of mixed Mn-Zr oxides: in situ XPS and XRD studies, Dalt. Trans. 44 (2015) 15499–15507. doi:10.1039/C5DT01440A.

[56] P. Pascuta, G. Borodi, N. Jumate, I. Vida-Simiti, D. Viorel, E. Culea, The structural role of manganese ions in some zinc phosphate glasses and glass ceramics, J. Alloys Compd. 504 (2010) 479–483. doi:10.1016/j.jallcom.2010.05.147.

[57] A. Gaddam, H.R. Fernandes, D.U. Tulyaganov, M.J. Pascual, J.M.F. Ferreira, Role of manganese on the structure, crystallization and sintering of non-stoichiometric lithium disilicate glasses, RSC Adv. 4 (2014) 13581. doi:10.1039/c3ra46393a.

[58] E. Regan, T. Groutso, J.B. Metson, R. Steiner, B. Ammundsen, D. Hassell, P. Pickering, Surface and bulk composition of lithium manganese oxides, Surf. Interface Anal. 27 (1999) 1064–1068. doi:10.1002/(SICI)1096-9918(199912)27:12<1064::AID-SIA676>3.0.CO;2-S.

[59] A. Goel, R.R. Rajagopal, J.M.F. Ferreira, Influence of strontium on structure, sintering and biodegradation behaviour of CaO-MgO-SrO-SiO2-P2O5-CaF2 glasses, Acta Biomater. 7 (2011) 4071–4080. doi:10.1016/j.actbio.2011.06.047.

[60] M.M. Azevedo, O. Tsigkou, R. Nair, J.R. Jones, G. Jell, M.M. Stevens, Hypoxia Inducible Factor-Stabilizing Bioactive Glasses for Directing Mesenchymal Stem Cell Behavior., Tissue Eng. Part A. 00 (2014) 1–8. doi:10.1089/ten.TEA.2014.0083.

[61] A.I. Caplan, Adult mesenchymal stem cells for tissue engineering versus regenerative medicine, J. Cell. Physiol. 213 (2007) 341–347. doi:10.1002/jcp.21200.

[62] F.F. Safadi, M.F. Barbe, S.M. Abdelmagid, M.C. Rico, R.A. Aswad, Bone Structure , Development and Bone Biology : Bone Pathology, in: Bone Pathol., 2009. doi:10.1007/978-1-59745-347-9_1.

[63] M. Khorami, S. Hesaraki, A. Behnamghader, H. Nazarian, S. Shahrabi, In vitro bioactivity and biocompatibility of lithium substituted 45S5 bioglass, Mater. Sci.

Eng. C. 31 (2011) 1584–1592. doi:10.1016/j.msec.2011.07.011.

[64] C. Wu, L. Xia, P. Han, L. Mao, J. Wang, D. Zhai, B. Fang, J. Chang, Y. Xiao, Europium-Containing Mesoporous Bioactive Glass Scaffolds for Stimulating in Vitro and in Vivo Osteogenesis, ACS Appl. Mater. Interfaces. 8 (2016) 11342–11354. doi:10.1021/acsami.6b03100.

[65] E. a Effah Kaufmann, P. Ducheyne, I.M. Shapiro, Evaluation of osteoblast response to porous bioactive glass (45S5) substrates by RT-PCR analysis., Tissue Eng. 6 (2000) 19–28. doi:10.1089/107632700320856.

[66] P.J. Thurner, C.G. Chen, S. Ionova-martin, L. Sun, A. Harman, A. Porter, J.W. Ager, R.O. Ritchie, T. Alliston, Osteopontin deficiency increases bone fragility but preserves bone mass, Bone. 46 (2010) 1564–1573. doi:10.1016/j.bone.2010.02.014.

[67] J. Isaac, J. Nohra, J. Lao, E. Jallot, J.M. Nedelec, A. Berdal, J.M. Sautier, Effects of strontium-doped bioactive glass on the differentiation of cultured osteogenic cells, Eur. Cells Mater. 21 (2011) 130–143.

[68] L.A. Strobel, N. Hild, D. Mohn, W.J. Stark, A. Hoppe, U. Gbureck, R.E. Horch, U. Kneser, A.R. Boccaccini, Novel strontium-doped bioactive glass nanoparticles enhance proliferation and osteogenic differentiation of human bone marrow stromal cells, J Nanopart Res. 15 (2013). doi:10.1007/s11051-013-1780-5.